Experimental CMB Status and Prospects: A Report from Snowmass 2001

Suzanne Staggs
*Princeton University**

Sarah Church
Stanford University†
(Dated: October 15th, 2001)

In recent years the promise of experimental study of the cosmic microwave background (CMB) has been demonstrated. Herein a brief summary of the field is followed by an indication of future directions. The prospects for further revelations from the details of the CMB are excellent. The future work is well-suited to the interests of high energy physics experimentalists: the projects seek to understand the fundamental nature of the universe, require subtle experimental techniques to keep systematics in control, produce large, rich data sets, and must be implemented by multi-institutional collaborations.

I. INTRODUCTION

The vast cache of information encoded in the CMB's intensity distribution has been tapped in recent years. In the last three years, a spate of independent experiments has evinced the primordial fluctuations present when the radiation decoupled from the matter at a redshift of $z \approx 1100$. Continuing measurements of the CMB temperature anisotropy should soon be joined by measurements of its polarization anisotropy. The polarization presents the enticing possibility of educing information about the inflation field itself. A third exciting area of CMB research is the measurement of its fine-scale anisotropy, at $\ell \gtrsim 2500$, where secondary effects dominate, so that the CMB serves as a backlight to illuminate dark parts of the universe. One of the main features of the fine-scale anisotropy is the Sunyaev-Zel'dovich effect in clusters, causing clusters to appear as either hot or cold spots, depending on the frequency of observation.

II. CURRENT STATUS OF TEMPERATURE ANISOTROPY MEASUREMENTS

Recent stunning results from the CMB have been measurements of its temperature anisotropy at angular scales between about 0.°2 and 2°. Data as of May, 2001, are plotted in the angular power spectrum of Figure 1, adapted from the compilation of Wang, Tegmark & Zaldarriaga (2001)[1]. The power spectrum clearly shows a peak near $\ell = 200$, and is consistent with the multiple peaks expected from oscillations of the primordial plasma at the time the radiation decoupled from matter. Much of the excitement generated by these data springs from the hope of fitting the measured power spectrum to determine fundamental cosmological parameters. An indication of the consistency of some of the recent larger data sets is provided in Table I, where parameters are estimated based on individual data sets.

TABLE I: Published results from fitting parameters to several recent large data sets, under the assumption of no gravitational waves. The table is based on one compiled by L. Knox.

Experiment	$\Omega_b h^2$	$\Omega_{cdm} h^2$	Ω_{tot}	n_s	Prior	Reference
DASI	$.022^{+.004}_{-.003}$	$.14 \pm .04$	$1.04 \pm .06$	$1.01^{+.08}_{-.06}$	$h > 0.45$; $\tau = 0$	[2]
BOOM	$.022^{+.004}_{-.003}$	$.13 \pm .05$	$1.02 \pm .06$	$0.96^{+.10}_{-.09}$	$0.4 < h < 0.9$	[3]
Maxima	$.030^{+.009}_{-.005}$	$.20^{+.10}_{-.05}$	$1.08^{+.16}_{-.04}$	$1.00^{+.12}_{-.15}$	$0.4 < h < 0.9$	[4, 5]

*Electronic address: staggs@princeton.edu
†Electronic address: schurch@stanford.edu

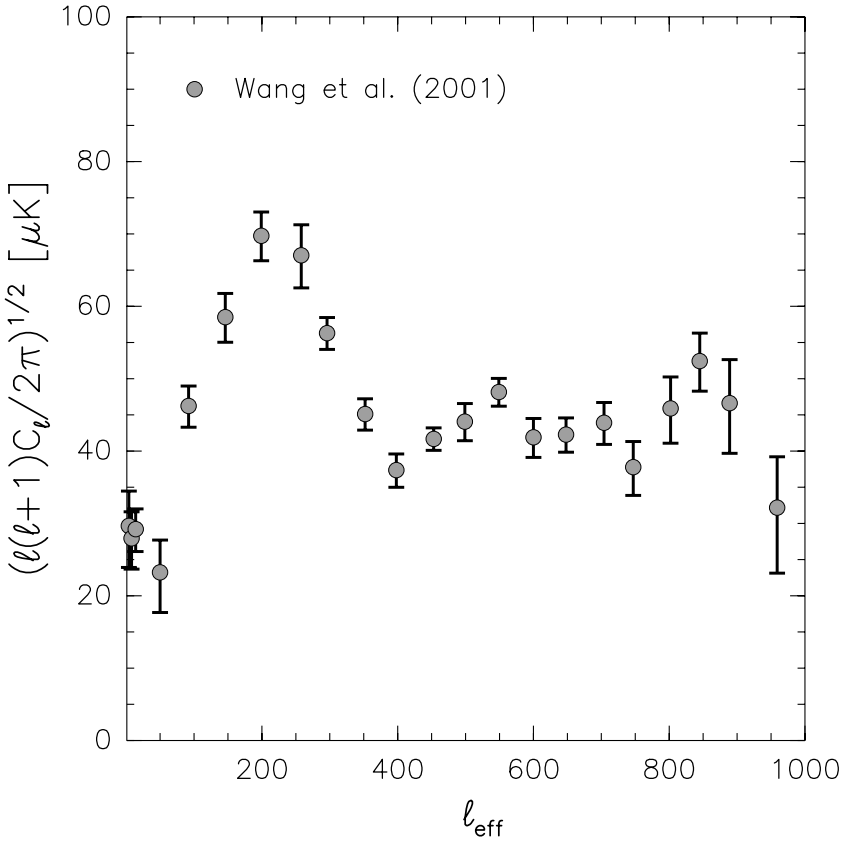

FIG. 1: The status of measurements of the temperature anisotropy angular power spectrum of the CMB as of May, 2001, based on the compilation of [1]. The authors binned 105 measurements of the power spectrum, including the effects of beam and calibration uncertainties. The individual measurements came from a variety of experiments, detailed by Wang, Tegmark & Zaldarriaga. Figure courtesy of M. Nolta.

A. Planned and Ongoing Temperature Anisotropy Experiments.

On the day before the Snowmass 2001 meeting began, on 30 June 2001, the Microwave Anisotropy Probe (MAP) was launched into space by NASA. The satellite has since reached its orbital position at L2, the saddle point four Earth-moon distances beyond the moon. Though by prior arrangement no results will be released for another year, the science team [6] reports that all systems are functioning well. The eponymous MAP will provide full-sky maps of the CMB fluctuations with high signal-to-noise measurements of the temperature power spectrum out to $\ell \approx 1000$, as indicated by the error boxes in Figure 2. The MAP data will reflect the advantages of a space mission: extreme control of systematic effects is possible, and the entire 4π of the sky can be measured.

In 2007, a second satellite will be launched: the Planck Surveyor which is a joint ESA/NASA mission. Planck will measure temperature fluctuations with high signal-to-noise out to about $\ell \approx 2000$, and will also measure polarization, as discussed below. See Figure 2 for estimates of Planck's sensitivity. It seems likely that after Planck, no other measurements of the CMB temperature power spectrum at $\ell < 2000$ will be needed.

Several other experiments are ongoing: DASI continues to collect data from the South Pole (though retooled to measure all four Stokes parameters now); Boomerang and Maxima each plan to fly again, to measure polarization as well as remeasure temperature anisotropy. CBI and ACBAR [7] have collected additional data, and MINT (a 140 GHz SIS-mixer-based four-element interferometer [6]) is presently deployed on the Chilean altiplano.

B. Concluding Remarks about the Temperature Anisotropy

The future looks bright for collecting definitive data on the power spectrum of the CMB out to $\ell \approx 2000$. Furthermore, large-scale, high-resolution maps of the CMB crucial for looking for nongaussian effects will soon

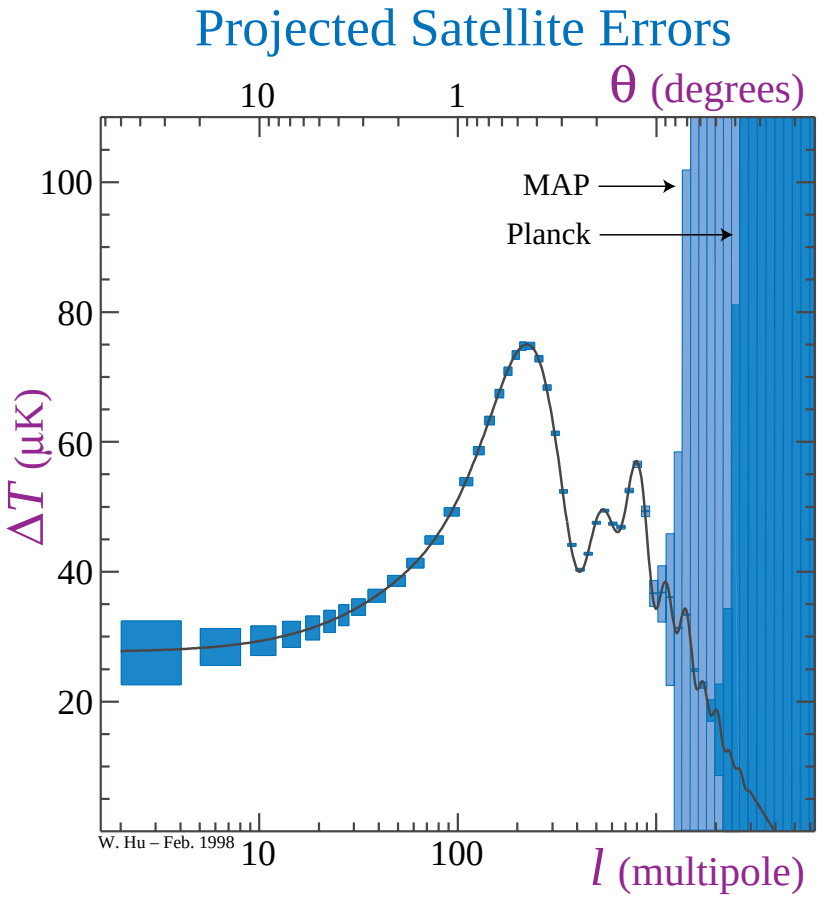

FIG. 2: Projected errors on the temperature anisotropy angular power spectrum for the CMB. Error boxes shown superimposed on a specific realization of the power spectrum represent estimates of the 1σ (68% CL) errors for measurements made at a given ℓ. The width of each box indicates the width of the "window function" used for averaging the data in that ℓ-bin. Figure courtesy of W. Hu.

be available. Published data already show good agreement among CMB experiments and consistency when pitted against other measurements of cosmological parameters. The days of making do with exiguous data are past.

III. CMB POLARIZATION EXPERIMENTS AND TECHNIQUES

The polarization of the CMB reveals more information about the universe than the temperature anisotropy can alone. However, the polarization is predicted to be about twenty times smaller than the temperature anisotropy. To date, no polarization anisotropy has been detected, though such detections should be imminent if rough theoretical predictions for its magnitude are correct (based on the sensitivities of ongoing and planned experiments).

The reader is referred to the report from the Snowmass working group P4 [8] for more details on the theoretical prospects for interpreting polarization data (as well as references for further reading). The polarization field is a tensor field which can be decomposed into a "curl" part and a "gradient" part, referred to as the B modes and the E modes, respectively. It turns out that the acoustic density and velocity perturbations which give rise to the bulk of the temperature anisotropy signal produce only E modes, while gravitational waves from the

inflation field itself can generate both E and B modes. Thus, detection of B modes could constrain inflation in a fundamentally new way.

Many of the techniques that have been used to detect temperature anisotropies in the CMB can be directly applied to measurements of CMB polarization. Additionally, polarization techniques from radioastronomy may be adapted. However, though the amplitude of E-mode polarization fluctuations is expected to be "only" twenty times smaller than the temperature anisotropies, the B-modes are likely to be ten times smaller still (see Fig. 3). Consequently, not only must the ultimate polarization experiments be of order 100 times more sensitive than current anisotropy experiments, they must also have 100 times better rejection of systematic signals.

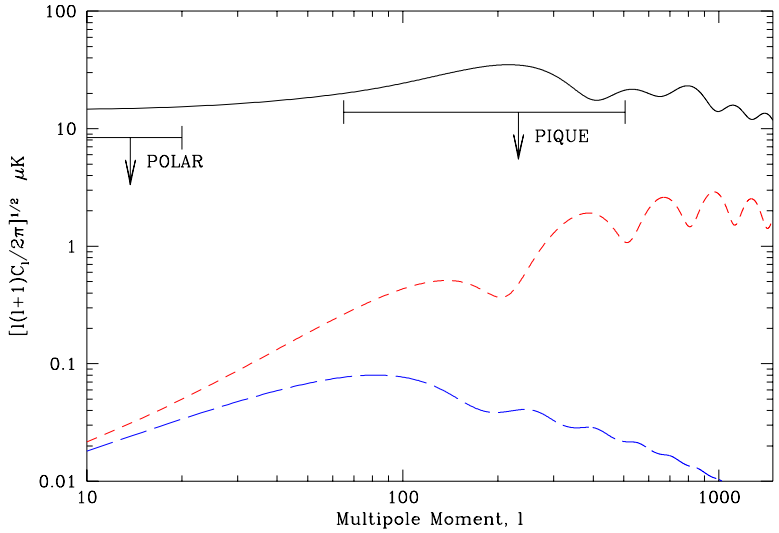

FIG. 3: Predictions for the power spectrum of the polarization of the CMB made using the CMBFAST code [9]. The assumed parameters in the model are $\Omega_b = 0.05$, Ω_{dm}=0.25, $\Omega_\Lambda = 0.7$ $n_S = 0.94$, $n_T = 0.94$, $Q_T/Q_S = 0.28$. Also shown are the best upper limits at $l < 1000$: POLAR[10] and PIQUE[11].

A. How to Measure Polarization

Rather than E and B, which are global properties of the radiation field, experiments measure the Stokes parameters describing its linear polarization: Q and U. (No circular polarization is predicted from primordial effects.) Of course, Q and U depend on the coordinate system chosen by the experimenters. Most experiments will require some modulation of the instrument coordinate system with respect to the sky ("chopping") to reduce systematic effects due to common-mode pick-up. Fortunately, as in the temperature case, prescriptions have been developed for using likelihood analysis on chopped Q and U data to constrain the power spectra of E and B. (See [12] and references therein, for example).

B. Detection Techniques

Just as with temperature anisotropy measurements, polarization measurement techniques fall in two types – coherent detection, in which the individual photons are amplified before detection, and incoherent detection, in which the photons are directly detected without amplification. Typically, measurements below 100 GHz are made with coherent techniques (high electron mobility amplifiers, or HEMTs), while those above are made with incoherent methods (bolometers). At 100 GHz, both techniques are feasible. At 150 GHz, SIS mixers provide another method of coherent amplification. The noise limitations of the two techniques are fundamentally different (see for example, [13]): bolometers are intrinsically more sensitive (and even more sensitive when used in a space environment with cooled optics). However, coherent techniques for rejecting large common-mode signals (ie, the intensity itself in this case) are well-understood from interferometry work. Also, HEMTs can be operated at temperatures of 4-20K allowing for relatively simple cryogenic systems based on mechanical cryocoolers. Bolometers need to be cooled to 300 mK or lower to realize high sensitivities. A final consideration is the problem of foregrounds: at frequencies below 100 GHz, polarized synchrotron radiation (with $T \propto \nu^{-\alpha}$ where $\alpha \sim 2.7$) is the primary contaminant, and above 100 GHz, polarized dust emission dominates.

C. Experimental Configurations

Both coherent and incoherent detection techniques are playing an important rôle in the search for CMB polarization. There are three types of experiments that are currently operating, or are under construction. The first two types (correlation polarimeters and interferometers) rely on phase-coherent correlations and thus are easiest to implement with coherent devices.

Correlation Receivers The best upper limits so far on CMB polarization have been obtained by the PIQUE [11] (at 90 GHz) and POLAR [10] (at 30 GHz) experiments (see Fig. 3). Both experiments use heterodyne correlation polarimeters, which employ phase-coherent techniques similar to those in interferometers. The key to the correlation polarimeter is that its output is directly proportional to one linear Stokes parameter: it does not require differencing of two large signals to a few parts in 10^7. One such polarimeter is shown schematically in Fig. 4. The signal from the sky is split into two orthogonal linear polarization states by an orthomode transducer (OMT). Each polarization state is then amplified by a HEMT amplifier. The radio frequency signals are down-converted to a lower frequency by mixing with a local oscillator. The two orthogonal polarization states are then multiplied together at the output of the receiver. Note that if the input axes are labeled x and y, then this polarimeter measures U, the linear polarization measured with respect to axes rotated by 45° to the x-y system.

The purpose of the phase switch, which periodically switches the phase of one branch of the LO between 0 and π, is to periodically reverse the sign of the output. This switching can take place at several kHz to modulate the output well above the $1/f$ noise from the amplifier. The result is extremely stable receivers: the $1/f$ knee of the PIQUE polarimeter was undetectable with measurements out to time scales of days.

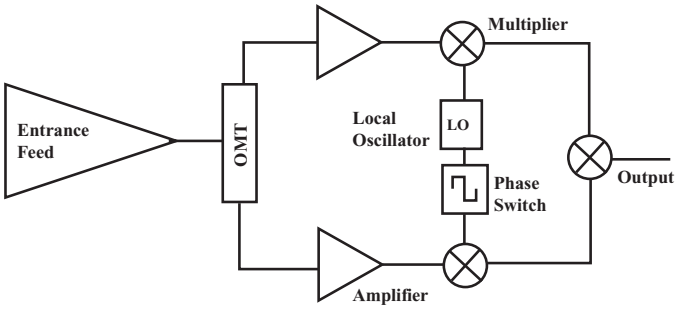

FIG. 4: Schematic of a correlation polarimeter. The phase switch in the local oscillator path multiplies the output by ±1 at kHz rates, well above the $1/f$ noise of the amplifiers. The output is proportional to the Stokes parameter U if the OMT axes define x and y.

HEMT technology is well-established and correlation receivers also have long track records in the radioastronomy community. The PIQUE and POLAR experiments are the first to demonstrate that systematic effects can be controlled to the few μK level for polarization measurements. However, the sensitivity of a coherent receiver is limited by the noise temperature of the amplifiers which cannot be lower than the quantum limit, $T = h\nu/k$. Consequently, at 100 GHz, for instance, a coherent receiver must add at least 5K of noise to the system. In practice, the best coherent receivers have noise temperatures about twice the quantum limit. The sensitivity of a coherent receiver may be quoted in terms of a noise equivalent temperature (NET; usually expressed in $\mu\mathrm{K}\sqrt{\mathrm{s}}$) which is given by:

$$\mathrm{NET} = f\frac{\sum_i T_i}{\eta\sqrt{\Delta\nu}}, \tag{1}$$

where the sum includes Rayleigh-Jeans equivalent temperatures for the CMB, the atmosphere, and the receiver (and any other incident noise). The factor f depends on details of the receiver; for a correlation receiver, $f = \sqrt{2}$. Here, $\Delta\nu$ is the bandwidth of the receiver and η is the system efficiency (typically > 0.95 for HEMT-based systems). For ground-based experiments, HEMT's are typically half as sensitive as bolometers. (Balloon-borne bolometers can be more than five times as sensitive as ground-based HEMTs, and the improvements in sensitivity for deployments in space are even more impressive.) A challenge for future experiments based on HEMTs will be to build the large focal plane arrays that will be needed to achieve the sensitivity required to detect B mode polarization. One avenue might be through monolithic microwave integrated circuit (MMIC) antenna-coupled HEMT correlation receivers.

Interferometric Techniques Some of the recent new data on the CMB temperature anisotropy has come from two interferometers operating in the 30-40 GHz range: DASI [14] and CBI [15] . Both have now been

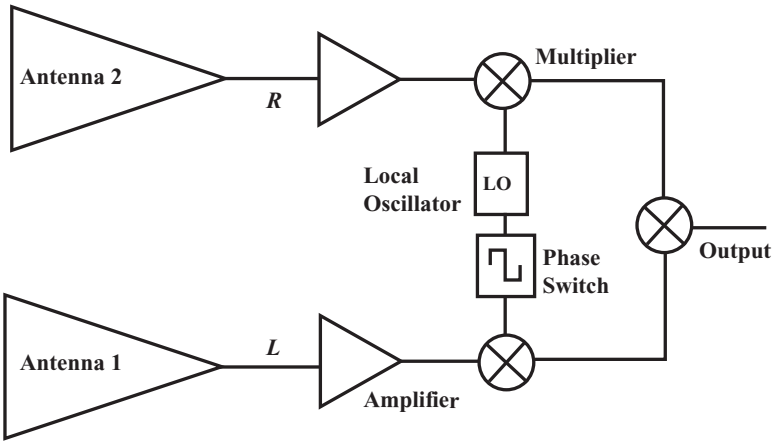

FIG. 5: Schematic of the correlation of one pair of antennas in an interferometer, meant to emphasize its similarity to the correlation polarimeter of Figure 4

reconfigured to make polarization measurements. As shown in Fig. 5, the instrumentation is similar to that in Fig. 4, but now the two inputs come from two antennas, rather than from the two arms of an OMT. Typically a single circularly polarized component of the radiation is amplified from each antenna. The outputs from each pair of antennas are correlated (multiplied together). Consequently the number of correlator channels required is proportional to n^2 where n is the number of antennas in the array. Inteferometers provide some immunity to local sources of systematics, including atmospheric emission and warm ground spillover. Like correlation polarimeters, when configured to measure polarization, interferometers do not have to difference two large signals to high accuracy; the correlation outputs are directly proportional to (linear combinations of) linear Stokes parameters. Interferometers also *directly measure* the power spectrum of fluctuations because each baseline is sensitive only to a narrow range of Fourier components of the sky brightness and thus to a narrow range of multipoles.

The sensitivity of an interferometer can be calculated from Equation 1 with:

$$f = \frac{\Omega_p}{\Omega_s} \frac{1}{\sqrt{n(n-1)}}$$

where Ω_p and Ω_s are the solid angles of a single antenna's beam (the field of view) and the synthesized beam, respectively.

Typically, to make polarization measurements, each antenna is configured to measure one component of *circular* polarization – either left (L) or right (R). Quarter-wave plates can be used to periodically switch each antenna between L and R states. This switching technique is implemented in DASIPOL [16]. All possible correlations between a pair of antennas – LR, LL, RR and RL – can be measured, from whence all four Stokes parameters may be determined, including V, the degree of circular polarization. The ability to measure I, Q and U quasi-simultaneously confers an important advantage to the interferometric technique. Interferometers can measure the temperature, polarization, and TE cross-correlation power spectra all with the same detector set. The primary disadvantage of an interferometer is that scaling it up to have a large number of detectors is challenging. The number of correlations grows as n^2 while the sensitivity grows as n. The state-of-the-art DASI and CBI instruments each have thirteen elements; to get ten times more sensitivity by a brute-force scaling up is impractical.

Direct Detection with Bolometers. Bolometers have been used with great success to measure the CMB anisotropy power spectrum as part of the balloon-borne Boomerang [17] and MAXIMA [18] experiments. Both are being reconfigured to observe polarization, and a number of other experiments that will use bolometers to measure polarization are also under construction (see Table II).

A bolometer comprises a thermistor attached to a substrate capable of absorbing photons (see Fig. 6). The photons heat the substrate, causing a temperature rise that is proportional to the absorbed power. The bolometer show in the lower panel of Fig. 6 has a substrate made of silicon-nitride etched into a "spider-web" pattern. This process removes most of the material, creating a sensitive, low heat-capacity structure, yet retains high optical efficiency because the gaps in the substrate are much less than a wavelength. The thermistor shown in the picture is neutron transmutation-doped germanium (NTD-Ge) which behaves as a temperature dependent resistor.

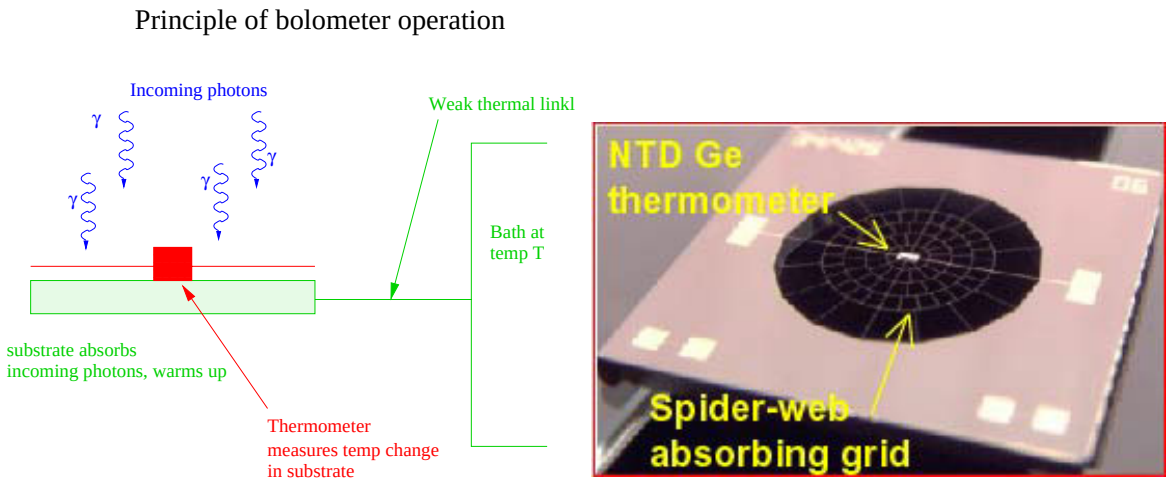

FIG. 6: Left: Principle of bolometer operation. Right: Picture of a silicon-nitride "spider-web" bolometer [Courtesy James Bock, Jet Propulsion Laboratory].

The sensitivity of a bolometer receiver may be described by a noise equivalent power (NEP; usually quoted in $\mathrm{W}/\sqrt{\mathrm{Hz}}$), which depends on the details of the thermistor, the substrate, the temperature and stability of the bath, the thermal coupling to the bath, and the readout electronics. In general, $\mathrm{NEP}^2 = \sum_i \mathrm{NEP}_i^2$, where the index i enumerates different sources of noise, including photon noise, Johnson noise, phonon noise, and other sources. (See the seminal work by John Mather: [19, 20].) Bolometers may be designed, constructed and operated such that the photon NEP dominates their noise; in that case they are said to have background limited performance (BLIP). The BLIP NEP for a bolometer with several sources P_i of power incident on it is given by:

$$\mathrm{NEP}_{\mathrm{BLIP}} = \sqrt{\sum_i [2P_i(h\overline{\nu} + \epsilon_i \eta_i k_B T_i)]},$$

where $\overline{\nu}$ represents the average frequency in the pass-band. Power sources incident on the detector may include the atmosphere, warm emission from the telescope and surroundings, and the CMB. The first term in parentheses is the contribution from random photon arrivals (shot noise due to Poisson statistics). The second term accounts for the effect of photon (boson) correlation and depends on the source emissivity ϵ_i and temperature T_i, and on the net efficiency through the optics to the detector, η. The NEP can be converted to an NET for comparison with a coherent receiver as follows:

$$\mathrm{NET} = \frac{1}{\sqrt{2\eta}} \frac{\mathrm{NEP}}{(\partial P_{\mathrm{CMB}}/\partial T_{\mathrm{CMB}})},$$

where η is the detection efficiency for CMB photons and P_{CMB} comes from the Planck radiation law. For example, the 300 mK spiderweb bolometers used by Boomerang [21] had typical NEPs of 3×10^{-17} $\mathrm{W}/\sqrt{\mathrm{Hz}}$, corresponding to a $\mathrm{NET}_{\mathrm{CMB}} \approx 200\mu\mathrm{K}\sqrt{\mathrm{s}}$. The best Maxima bolometers (100 mK) had $\mathrm{NET}_{\mathrm{CMB}} \approx 100$ $\mu\mathrm{K}\sqrt{\mathrm{s}}$ [22]. For comparison, the best QMAP HEMT-based receiver had a sensitivity of 400 $\mu\mathrm{K}\sqrt{\mathrm{s}}$ [23].

Bolometers are not intrinsically sensitive to the polarization state of the incoming radiation. Linear components of the radiation field can be selected by (i) placing wire-grid polarizers in front of the bolometer, (ii) using an OMT and then detecting the two linear polarization modes with separate bolometers, or by (iii) making the bolometer substrate itself polarization sensitive by a suitable choice of geometry for the substrate. Future experiments will use all three methods.

Bolometers respond equally well to *all* frequencies. Consequently the radiation must be carefully filtered before it reaches the bolometer. Fig. 7 shows how a bolometer is coupled to a telescope. Metal-mesh resonant grid filters define a pass-band with high transmission and low out of bands leaks [24]. Typically the structure shown in the figure has a transmission efficiency of 40% [25].

Figure 8 shows schematically how this structure can be adapted to measure polarization. In the top panel, an OMT is used to split the signal into two orthogonal components which are then detected by separate bolometers [26]. In the bottom panel, two separate feeds are used to measure orthogonal components by placing a wire polarizing grid in front of each feed.

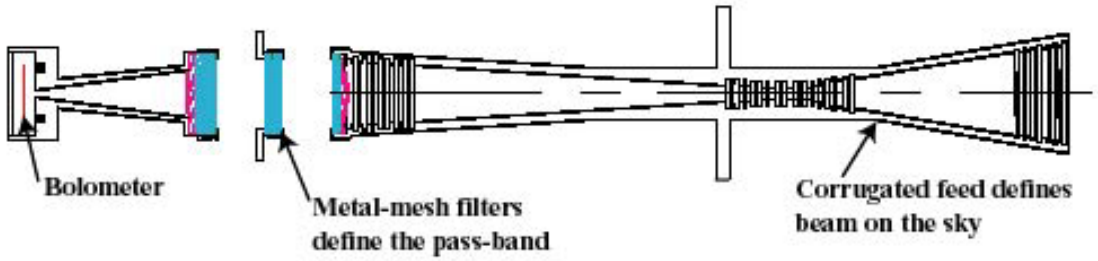

FIG. 7: Schematic showing how a bolometer is coupled to the sky.

To measure Q and U, the outputs of two bolometers are differenced. Pairs of bolometers must be well-matched to allow rejection of the common-mode signal which is 10^{6-7} times larger than the signals of interest. (Alternatively, mechanical rotation of either a grid or a quarter-wave plate allows linear Stokes parameters to be measured by a single bolometer; these techniques have their own technical problems.) The SuZIE measurements have successfully differenced matched pairs of bolometers [27]. If the instrument coordinate system is at an angle θ to the sky coordinate system, the output from the receiver is proportional to $[Q\cos 2\theta + U \sin 2\theta]$. Rotating the receiver thus provides good systematic checks. Ideally, to minimize systematics, the two bolometers should simultaneously view the same pixel on the sky. Although this can be achieved by using OMTs, the resulting architecture is bulky, limiting the number of feeds that can be packed into a focal plane. A more compact method recently developed replaces the dual-polarization bolometer in Figure 7 with a polarization sensitive bolometer (PSB): two vertically stacked bolometers each sensitive to one of two orthogonal linear components of the radiation. Both approaches will soon be tested – the Polatron experiment uses an OMT [26], and a new flight of Boomerang will provide the first data from PSBs.

There are good prospects for developing large focal plane arrays of bolometers. BOLOCAM [28] already comprises 151 detectors. The NTD Ge thermistors can be replaced with photolithographed transition edge superconductor [29, 30]. Recent submm instruments based on "pop-up" detectors (bolometers whose leads are folded down out of the focal plane to allow close-packing) have demonstrated new multiplexing techniques [30, 31] which will be critical for coping with large numbers of detectors.

D. Current Status of the Field

Current experiments have as their first goal detection of the E-modes of polarization. Table II provides a summary of all experiments that are observing, or under construction, or in the proposal stage.

Technology Requirements for Future Polarization Experiments. Both HEMTs and bolometers are state-of-the-art in the sense of being as sensitive as is allowed by fundamental limitations. Consequently we cannot expect substantial improvements in the performance of a single detector alone to improve the limits on polarization. The only way to achieve the sensitivities required is to have many (perhaps tens of thousands) such detectors. In addition, the ideal polarization experiment also needs:

- The ability to integrate for many months without encountering systematic effects.
- A wide range of observing frequencies to remove astrophysical foregrounds from, for example, synchrotron, free-free and dust emission (see Section III F).

Significant developments are likely in both areas, especially on the bolometer side, as discussed in Section III C. The main barrier in both cases is the cost of development. These technologies are, in general, beyond the scope of the small groups that have traditionally performed CMB experiments. The new generation of bolometer arrays are being built in government labs (JPL, NASA Goddard and NIST, for example) which are traditionally limited in the types of applications they can support and which cannot in general support ground-based applications. As discussed below, ground-based experiments represent the best strategy for testing various techniques prior to designing a satellite. Consequently a challenge facing the community is how to fund the development of these expensive arrays.

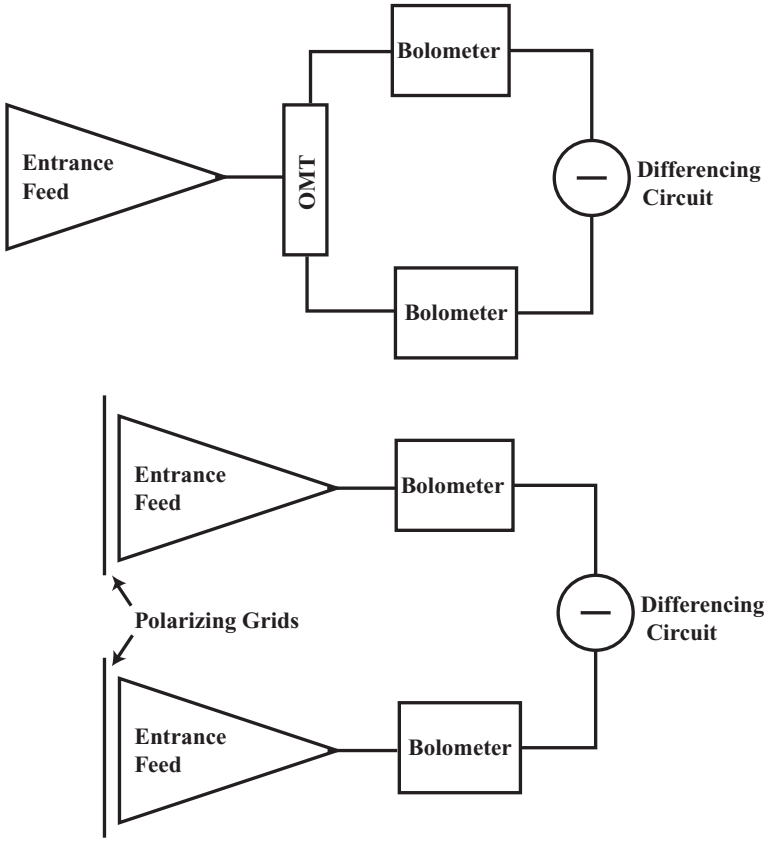

FIG. 8: Two ways in which bolometers can be used to measure polarization.

Ground vs Space A CMB experiment that is specifically designed to measure B-mode polarization will require significant advances in technology over and above that which will fly on the Planck Surveyor. Additionally, the observing regime is completely new in terms of the required sensitivity and freedom from systematics – we simply do not yet know how to optimize an experiment that must be orders of magnitude better than the best available right now. For this reason, it is prudent to start first with ground-based experiments which are naturally able to observe for many months, which are cheap and easy to build, and which can be easily reconfigured to take advantage of new advances in technology. Of course, in the near term we also look forward to exciting results from the balloon-borne B2K (Boomerang with PSBs) and MAXIPOL.

Advocating an initial round of ground-based measurements might seem to conflict with the traditional "space is best" view in the CMB community. The time-varying atmospheric emission, which additionally has spatial structure, hampers ground-based measurements of the temperature anisotropy. Spatial switching at frequencies much higher than the atmospheric time scales has been used with great success [23], as has interferometry [14, 15], but the lowest multipoles, where B modes may dominate, are lost. However, the atmospheric emission is believed to be unpolarized [32]. Thus, ideal polarimeters are insensitive to fluctuations in the atmosphere. In practice, all polarimeters have some finite response to the common mode (the intensity I), so rejecting atmospheric fluctuations with some form of spatial switching is likely to be necessary to get residual pickup down to the sub-μK level. Nonetheless, the relative insensitivity of polarization experiments to atmospheric problems is a decided advantage.

E. Minimizing Systematic Effects

Measuring even E-modes of polarization will require an instrument with high sensitivity and good control of systematics. Systematic effects include the known ones associated with CMB temperature anisotropy measurements and some new effects that are specific to polarimetry. A review of these effects and their effects on bolometric detector systems can be found in [26]. We summarize the main effects below (excluding atmospheric emission, discussed above).

	Detectors	Freq./GHz (No of focal plane elements)	Beam	Platform	Primary Mirror
Completed:					
POLAR	HEMTs	30(1)	7°	Ground	None
Observing:					
CBI Interferometer	HEMTs	26-36 (13)	3′	Ground	On-axis
COMPASS	HEMTs	30(1), 90(1)	20′, 7′	Ground	On-axis
DASI Interferometer	HEMTs	36-46 (13)	20′	Ground	None
MAP	HEMTs	22(2), 30(2), 40(4), 60(4), 90(8)	13′–1°	Space	Off-axis
PIQUE	HEMTs	40(1), 90(1)	30′, 15′	Ground	Off-axis
Under Construction:					
CAPMAP	HEMTs	40(4), 90(10)	6′, 3′	Ground	Off-axis
B2K	Bolometers	150(4), 240(4), 350(4)	12′	Balloon	Off-axis
Maxipol	Bolometers	150(12), 420(4)	10′	Balloon	Off-axis
Planck LFI	HEMTs	30(2), 44(3), 70(6), 100(17)	10′–33′	Space	Off-axis
Planck HFI	Bolometers	150(4), 220(4), 350(4)	6′	Space	Off-axis
Polatron	Bolometers	100(1)	2.5′	Ground	On-axis
QUEST	Bolometers	100(12), 150(24), 220(19)	6.5′-3′	Ground	On-axis
AMIBA Interferometer	HEMTs	90(19)	2′	Ground	On-axis
SPORT	HEMTs	22, 32, 60, 90	7°	Space	None
Proposed:					
Bar-SPORT	HEMTs	32, 90	30′, 12′	Balloon	Unknown
POLARBEAR	Bolometers	150(3000?)	10′	Ground	Off-axis

TABLE II: Status as of July 2001 of current and planned polarization experiments. Note that for the interferometers, each element receives either right or left circular polarization at any instant. Also note that for all detectors on Maxipol, and for the detectors at the two higher frequencies for B2K, each detector receives only one of the two orthogonal polarization modes.

Ground Spillover. Warm emission from the ground can be reflected into an instrument by diffraction around the mirrors or scattering from the mirror support structures, particularly for on-axis systems. Diffraction is a polarization-dependent process, and thus partially polarizes the incoming radiation. The most sensitive measurements of CMB anisotropies to date have either used interferometric techniques which reduce spillover by shifting it to a frequency well away from the fringe frequency, or off-axis mirrors which minimize the blockage of the primary aperture and consequently have very low spillover. The detectors are fed with carefully designed feed optics (usually corrugated feeds which have very low sidelobes) that maximize the illumination of the primary mirror while maintaining very low ground spillover.

However, off-axis mirrors both generate polarized emission (which will vary slowly in time unless all mirrors are temperature-controlled), and increase the degree of instrumental polarization (see below). For that reason, some groups are returning to the use of on-axis Cassegrain telescopes, even though these systems have increased spillover due to the blockage of the mirrors and a smaller field of view. Deciding on paper which approach is best is a difficult exercise. The definitive answer will come from the next generation of experiments since, as shown in Table II, both approaches are being adopted by different groups.

Instrumental (Systematic) Polarization. Instrumental polarization occurs when an unpolarized signal at the input of the telescope generates a polarized signal at the output. In other words, it is a means of reducing the common mode rejection of the system. It is usually the result of a mismatch in the transmission of the two orthogonal polarization modes that are being differenced, and is generally enhanced by off-axis reflections.

Cross-polarization Cross-polarization occurs if there is cross-talk between the two orthogonal polarization modes. The effect is to reduce the amplitude of a polarized signal and so this effect is also called polarization efficiency. A well-designed experiment should achieve 1% or less cross-polarization.

F. Foregrounds

Foregrounds are potentially a major source of uncertainty in polarization measurements, just as they are in temperature anisotropy measurements. Comprehensive reviews of foregrounds and their likely contribution to

both temperature and polarization anisotropies can be found in [33], [34]. The simulations in [34] show a minimum in the amplitude of polarized foregrounds at 100GHz, which is why most of the polarization experiments include this channel. There remains considerable uncertainty in the amplitude of foregrounds, mainly due to a lack of polarized maps of large areas of sky at a wide range of frequencies. Because of this, the ideal experiment will observe at a range of frequencies to allow foreground removal based on spectral information.

G. Conclusions

The next few years will see data from a large number of CMB experiments which will use a variety of different techniques and which will be subject to different systematic effects. These experiments should measure the TE cross-correlation and obtain the first estimates of the E mode power spectrum. Moreover, there is still a lot that can be accomplished from the ground and from balloon, and the technology development that will eventually lead to the ultimate experiment requires us as a community to move away from the "traditional" single university-based experiment.

The ultimate goal of polarization experiments is a measurement of both E and B mode polarization to the limit set by cosmic variance. This will require a new generation of experiments with many thousands of background limited detectors, eventually on a space-based platform. However, we conclude that competing design philosophies are best tested on the next generation of ground and balloon-based experiments. These experiments are beginning to approach cost and complexity levels that are too great to allow the CMB community to continue easily in the few-investigator mode that has worked so well for the temperature anisotropy measurement program. The challenge for our community is to develop collaborations and sources of funding that will allow us to proceed to the next generation of CMB measurements.

IV. FINE-SCALE CMB AND SUNYAEV-ZEL'DOVICH EXPERIMENTS

A. The Promise of Fine-scale CMB Measurements.

Measurements of the CMB temperature anisotropy at arcminute angular scales ($\ell > 2000$) can reveal still more about the Universe's fundamental nature. The dominant contribution to anisotropies at these fine scales is not the primordial (or intrinsic) signal reflecting conditions at the surface of last scattering, but is instead the Sunyaev Zel'dovich (SZ) effect [35]. The SZ effect has a frequency signature which allows it to be disentangled from primordial CMB anisotropies. Other interesting effects include the generation of distinctive non-Gaussianities by gravitational lensing, the contribution from CMB photons scattered off *moving* electrons after the epoch of reionization (the Ostriker-Vishniac effect), and the contribution from the kinetic SZ effect (see below.)

Science from the SZ Effect. The SZ effect arises from the Compton scattering of CMB photons from hot electrons in CMB with ionized gas along a line-of-sight to the surface of last-scattering. The hottest gas is located in the potential wells of rich galaxy clusters where the gas temperature ranges from 2–15 keV. The SZ effect is *independent of the redshift of the ionized gas* and thus provides a prime technique for detecting clusters of galaxies out to the epoch of cluster formation. (Distant clusters are typically too faint to be seen with X-ray measurements.) We refer the reader to the report from the Snowmass 2001 P4.1 working group [8] for an overview of the exciting cosmology possible from a large SZ-selected sample of clusters. If a cluster has a peculiar velocity with respect to the rest frame of the CMB, the "kinetic SZ effect" may also be measured in principle, allowing estimation of the dark matter content of the Universe from maps of the large scale dynamics of the clusters.

Notice that the CMB acts as a uniform backlight to *all* of the hot gas in the universe, including the cooler, less-dense gas with temperature 8–800 eV which is predicted from simulations of large scale structure formation to exist as a filamentary structure between clusters [36].

Quantifying the SZ Effect. Compton-scattering of CMB photons by the much hotter electrons in the gas causes a distortion, $\Delta I_{\rm th}$ to the intensity, $I_{\rm CMB}$, which in the non-relativistic limit is given by:

$$\begin{aligned} \frac{\Delta I_{\rm th}}{I_{\rm CMB}} &= \frac{x e^x}{(e^x-1)}\left[x\coth\frac{x}{2}-4\right] y_{\rm th}, \text{ where} \\ y_{\rm th} &= \sigma_T \int n_e \frac{kT_{\rm e}}{m_{\rm e}c^2}{\rm d}l, \end{aligned} \tag{2}$$

and where $x = h\nu/kT_{\rm CMB}$. The quantity $y_{\rm th}$ is proportional to the pressure of the gas integrated along the line-of-sight to the last scattering surface and depends on $T_{\rm e}$, the temperature of the gas, σ_T, the Thompson

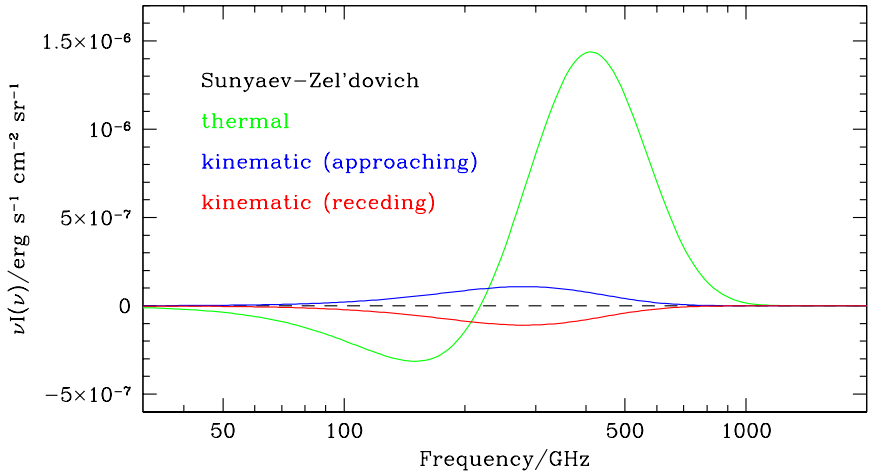

FIG. 9: Brightness of the SZ effect as a function of frequency. The solid line is the thermal component, and the two dotted lines show the kinetic component. The sign of the kinetic component depends on the direction of the cluster peculiar velocity relative to the observer. The assumed parameters are $\tau = 0.01$, $T_e = 5$ keV, and $v_{\rm pec}$=1000 km/s.

cross-section, and n_e, the electron density. The distortion characterized by $y_{\rm th}$ is known as the thermal SZ effect because the amplitude is related to the thermal motions of the electrons in the clusters. The thermal SZ effect has a unique spectral shape (see Fig. 9) causing a rich cluster to appear as a "hole" in the CMB at frequencies $\nu < \nu_{\rm NULL}$, but as a hot spot at $\nu > \nu_{\rm NULL}$, where the null frequency is $\nu_{\rm NULL} \sim 217$ GHz. (Note that relativistic corrections to Eq. 3 alter the spectrum slightly so that the null frequency depends weakly on the gas temperature [37, 38].)

The kinetic SZ effect arises from the bulk motion of the cluster plasma in the rest frame of the CMB. The change in brightness is given by

$$\frac{\Delta I_{\rm kin}}{I_{\rm CMB}} = \frac{x e^x y_{\rm kin}}{(e^x - 1)}, \text{ where} \qquad (3)$$
$$y_{\rm kin} = \sigma_T \int n_e \frac{\mathbf{v}_{\rm pec} \cdot \mathrm{d}\mathbf{l}}{c} = \tau \frac{v_{\rm pec}}{c}.$$

Here $v_{\rm pec}$ is the mean radial component of the peculiar velocity of the cluster plasma, $\mathbf{v}_{\rm pec}$. The optical depth, τ, of a rich cluster is typically 1%. The spectral profile of the kinematic SZ effect is also shown in Figure 9. The kinematic effect has yet to be detected, but for expected cluster peculiar velocities of a few hundred km/s, it is likely to be at least an order of magnitude fainter than the thermal effect.

The expressions in Eqs. 3 and 4 give the SZ effect along a given line of sight through a cluster, This quantity has *no explicit redshift dependence* because both ΔI and $I_{\rm CMB}$ scale in the same way with redshift. Consequently, the amplitude and spectral shape of the SZ effect are independent of the distance to the cluster. Of course, the redshift does affect the total SZ flux from a cluster, through geometrical effects [39–41]. These redshift dependencies are much weaker than for other sources of emission such as X-ray measurements.

B. Current and Future Experimental Prospects

Table III shows current and future experiments intended to measure the SZ effect.

Current Status of SZ Measurements. Detections of the thermal SZ effect are now routine (see [46] for a review) and have reached the level where SZ measurements may be used as important cosmological probes.

Figure 10 shows high quality data obtained from mm-wave interferometers outfitted with 30 GHz receivers [47] and the SuZIE instrument. Several low sky coverage surveys to look for clusters have been carried out. However to obtain the large numbers of clusters out to a reasonably small limiting mass (for example, 3-4 $\times 10^{14} M_\odot$) required for setting new constraints on cosmology, experiments capable of surveying large portions of the sky to high sensitivity are needed.

Detection Techniques. SZ survey instruments fall into two categories: HEMT-based interferometers at 30-40 GHz, observing clusters by their "SZ decrement," and bolometer arrays with multiple frequency bands straddling the null frequency coupled to large telescopes. Many of the comparisons between coherent and incoherent techniques made in Section III G apply here also. Atmospheric fluctuations hamper the bolometer

Name	Type	N_{det}	ν (GHz)	N_{ch}	FOV	Res	Status	Site/Date
ACBAR [7, 42]	Bolo	16	150–345	4	1.5°	5′	operating	SP/2001
BOLOCAM [28]	Bolo	151	130–250	1	···	0.6′–1.1′	operating	CSO/2001
AMiBA [43]	Int	19	90	1	11′	2.6′	building	···/2003
AMI [44]	Int	10	15	1	21′	4.5′	building	UK/2003
SZA [16]	Int	8	30,90	2	12′, 4′	1.5′	building	OVRO/2003
ACT/MBAC [6]	Bolo	3072	145–265	3	22′	0.9′–1.7′	proposed	Chile/2004
SPT/BA [16]	Bolo	1024	150-220	2	1°	1.3′	proposed	SP/2005
Planck/HFI [45]	Bolo	50	100-580	6	···	5′	building	space/2007

TABLE III: Comparison of current and planned experiments making SZ cluster surveys. The second column distinguishes interferometer experiments from experiments coupling bolometer arrays to large telescopes. The fifth column gives N_{ch}, the number of frequency channels, while the sixth and seventh columns give the FWHM of the field of view and the beam (resolution), respectively. Note that the ACBAR FOV is obtained by chopping their bolometer array 3° on the sky. See the text for an indication of mapping speeds. At present, only ACBAR, ACT/MBAC, SPT/BA, and Planck/HFI plan to collect data at all frequency channels simultaneously. Not included here is the extended SZA, which adds in the 6 (larger) BIMA telescopes to form a heterogeneous interferometer, providing for even better removal of radio point sources.

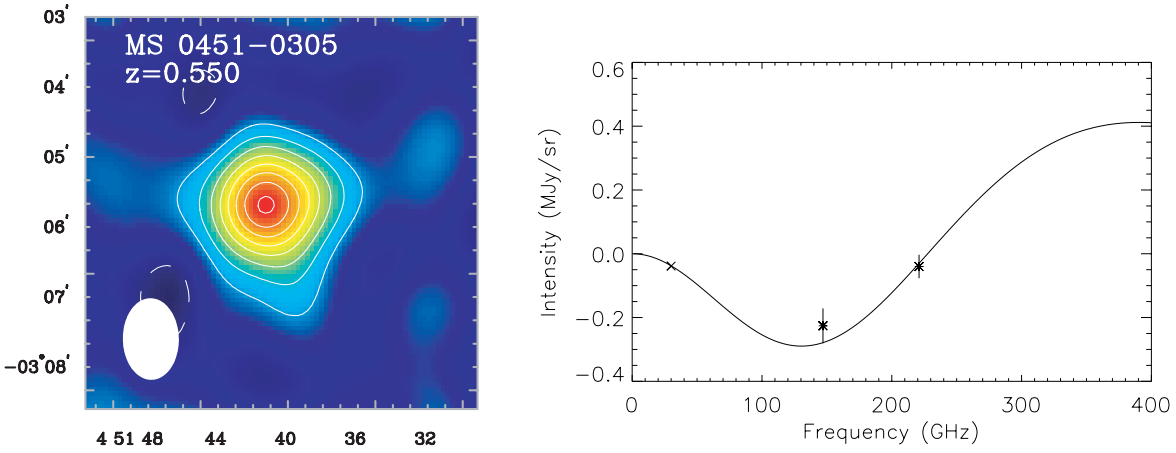

FIG. 10: Upper Panel: Map of the SZ decrement towards the high redshift cluster MS0451 made using the BIMA array (courtesy J. Carlstrom.). Lower Panel: Measurement of the spectrum of MS0451 using the flux measured with the BIMA array (cross) and the SuZIE experiment (stars).

experiments more than the interferometers, but such fluctuations are smaller at the angular scales of interest than they are near the peak of the CMB temperature angular power spectrum. At a good site (Chile, South Pole, Mauna Kea), the atmosphere will not be a limiting factor for more than 50% of the time. An additional consideration here is that interferometers suffer from not being able to spectrally distinguish SZ sources; if their resolution is $\gtrsim 2'$, survey mass limits are set by confusion from the intrinsic CMB anisotropies. On the other hand, interferometers can make beautiful maps of the clusters (as in Figure 10), allowing detailed study of the clusters which will provide critical guidance for extracting cosmological goals from cluster surveys.

Therefore, both approaches should be pursued, and, as Table III indicates, experiments of both types are already underway. The table omits comparison of mapping speeds for fear of misrepresenting the instruments. Note that mapping speeds are given in units of $\mathrm{deg}^2/(\mathrm{K/beam})^2/\mathrm{s}$, and thus quantify how much sky coverage can be mapped to a given sensitivity per pixel ("beam") in how much time. Golwala [48] notes that the mapping speed for a bolometer array is given by $\Omega_b N_{det}/\mathrm{NEy}^2$, while for an interferometer, it is $\Omega_{\mathrm{FOV}}/\mathrm{NEy}^2$. Here, Ω_b and Ω_{FOV} are the solid areas of the beam and field of view (FOV), while the noise equivalent y is $\mathrm{NEy} = \alpha(\nu)\mathrm{NET}$, with the NET for a single detector. The proportionality α accounts for the fact that the spectral distortion for the SZ effect from a cluster is larger at frequencies away from the null. At 30 GHz, $\alpha \sim 0.0002$, while at 150 GHz, $\alpha \sim 0.35$. A rule of thumb is that on the ground, bolometer NETs are comparable to the best HEMT amplifier NETs at 30-40 GHz (to within a factor of two).

Future Prospects. Realizing the full science potential from SZ-selected cluster samples requires a large number of clusters with redshift information obtained after their detection in the SZ survey. Therefore, very

sensitive instruments are required, with large numbers of detectors. Thus, both future CMB polarization experiments and SZ survey experiments require development of large multiplexed arrays of bolometers. Luckily, the technology is coming online already (e.g. [31]), and with continued funding, is likely to be ready when we are – after the first data come in from the existing generation of polarization and SZ-survey instruments.

V. CONCLUSIONS

Recent measurements of the CMB temperature anisotropy hang together with other cosmological data to give a consistent picture of our universe as spatially flat, dominated by a Λ-like term, and with 5-10 times more dark matter than baryons (by mass).

These published CMB data are just the beginning. In the near future, the MAP satellite data set will be a gold mine: full-sky maps in five frequency bands, with the very stringent control of systematic effects that only the space environment permits. The Planck data toward the end of the decade will be even richer, with twice the angular resolution and broader frequency coverage.

Beyond measuring the primary temperature anisotropy of the CMB lie the next two exciting frontiers: the CMB polarization and the fine-scale structure of the CMB's intensity (including SZ cluster surveys). Definitive measurements of both these aspects of the CMB require experimental sensitivities at least an order of magnitude better than have yet been achieved. Individual detectors are near enough fundamental limits to their sensitivities that the only feasible route to progress on these two fronts is through large arrays of detectors. Here, "large arrays" is a term encompassing bolometer arrays, interferometric arrays, and HEMT-receiver-on-a-chip arrays. Experiments with large arrays require significant funding, substantial technical development, and therefore, sizeable collaborations. At the same time, more modest "stepping-stone" experiments will be crucial for exploring the new systematic effects revealed when the statistical errors are reduced. Smaller experiments are faster and more flexible, and thus can inform the designs of large-array collaborations in a timely way.

Acknowledgments

We would like the thank all the attendees who contributed to this workshop. In particular we thank Sunil Golwala, Peter Timbie, and Lloyd Knox for allowing us to use materials from their presentations herein.

[1] X. Wang, M. Tegmark, and M. Zaldarriaga, (2001), astro-ph/0105091.
[2] C. Pryke *et al.*, (2001), astro-ph/0104490.
[3] C. B. Netterfield *et al.*, submitted to ApJ(2001), astro-ph/0104460.
[4] A. Balbi *et al.*, Astrophys. J. Lett.**545**, L1 (2000).
[5] A. Balbi *et al.*, Astrophys. J. Lett.**558**, L145 (2001).
[6] L. A. Page, (private communication), 2001.
[7] W. L. Holzapfel, (private communication), 2001.
[8] S. Church, A. Jaffe, and L. Knox, (2001), to appear in *report from Snowmass 2001: The Future of Particle Physics, astro-ph/0111203*.
[9] U. Seljak and M. Zaldarriaga, ApJ**469**, 437 (1996).
[10] B. G. Keating *et al.*, Astrophys. J. Lett.**560**, L1 (2001).
[11] M. M. Hedman *et al.*, Astrophys. J. Lett.**548**, L111 (2001).
[12] M. Zaldarriaga, ApJ**503**, 1 (1998).
[13] J. Zmuidzinas, in *The Physics and Chemistry of the Interstellar Medium*, edited by V. O. et al. (GCA-Verlag, Herdecke, 1999), pp. 423–430.
[14] E. M. Leitch *et al.*, (2001), astro-ph/0104488.
[15] S. Padin *et al.*, ApJ**549**, L1 (2001).
[16] J. E. Carlstrom, (private communication), 2001.
[17] P. de Bernardis *et al.*, Nature **404**, 955 (2000).
[18] S. Hanany *et al.*, Astrophys. J. Lett.**545**, L5 (2000).
[19] J. Mather, Appl. Opt. **21**, 1125 (1982).
[20] J. Mather, Appl. Opt. **23**, 584 (1984).
[21] F. Piacentini *et al.*, (2001), astro-ph/0105148.
[22] A. T. Lee *et al.*, in *3K Cosmology*, edited by L. Maiani, F. Melchiorri, and N. Vittorio (AIP Conference Proceedings 476, College Park, MD, 1999).
[23] A. D. Miller *et al.*, (2001), astro-ph/0108030, submitted to ApJ.

[24] C. Lee, P. Ade, and C. Haynes, *30th ESLAB Symposium: Submillimetre and Far-Infrared Space Instrumentation* (ESA Publications Division, Noordwijk, The Netherlands, 1997), Vol. SP-388, p. 77.
[25] S. Church *et al.*, *30th ESLAB Symposium: Submillimetre and Far-Infrared Space Instrumentation* (ESA Publications Division, Noordwijk, The Netherlands, 1997), Vol. SP-388, p. 77.
[26] B. Philhour *et al.*, submitted to ApJ(2001), astro-ph/0106543.
[27] W. L. Holzapfel *et al.*, ApJ**497**, 17 (1997).
[28] http://lmtserver.phast.umass.edu/pub/Documents/010/.
[29] A. Lee *et al.*, Appl. Phys. Lett. **69**, 1801 (1996).
[30] D. J. Benford *et al.*, Int. J. IR MM waves **21**, 1909 (2000).
[31] D. J. Benford *et al.*, (2001), from the 9th Workshop on Low Temperature Detectors, *AIP proceedings*, in press.
[32] B. Keating, P. Timbie, A. Polnarev, and J. Steinberger, ApJ**495**, 580 (1998).
[33] F. R. Bouchet, R. Gispert, and J. L. Puget, in *Unveiling the Cosmic Infrared Background*, edited by E. Dwek (AIP Conference Proceedings 348, Baltimore, 1996).
[34] M. Tegmark, D. Eisenstein, W. Hu, and A. de Oliveira-Costa, ApJ**530**, 133 (1999).
[35] R. Sunyaev and Y. B. Zel'dovich, Comments Ap. Space Phys. **4**, 173 (1972).
[36] R. Cen and J. Ostriker, ApJ**514**, 1 (1999).
[37] S. Nozawa, N. Itoh, Y. Kawana, and Y. Kohyama, ApJ**536**, 31 (2000).
[38] Y. Rephaeli, ApJ**371**, L1 (1995).
[39] D. Barbosa, J. G. Bartlett, A. Blanchard, and J. Oukbir, A&A **314**, 13 (1996).
[40] G. P. Holder and J. E. Carlstrom, ApJ**558**, 515 (2001).
[41] L. Verde, Z. Haiman, and D. N. Spergel, submitted to ApJ(2001), astroph/0106315.
[42] http://astro.uchicago.edu/cara/research/cmbr/acbar.html.
[43] http://www.asiaa.sinica.edu.tw/amiba/.
[44] http://www.mrao.cam.ac.uk/telescopes/ami.
[45] http://astro.estec.esa.nl/SA-general/Projects/Planck/.
[46] J. Carlstrom *et al.*, Physica Scripta, volume T **85**, 148 (2000).
[47] J. E. Carlstrom, M. Joy, and L. Grego, Astrophys. J. Lett.**456**, 75 (1996).
[48] S. Golwala, (private communication), 2001.